

RAPID COMMUNICATION

Laser-induced phase conversion of n-type SnSe₂ to p-type SnSe

To cite this article: Qi Zheng *et al* 2022 *Chinese Phys. B* **31** 047306

View the [article online](#) for updates and enhancements.

You may also like

- [Two-step fabrication of single-layer rectangular SnSe flakes](#)
Jizhou Jiang, Calvin Pei Yu Wong, Jing Zou *et al.*
- [A Low Temperature NO₂ Sensor Based on SnSe₂/SnO₂ Heterojunction](#)
Baoyu Huang, Xinyu Li and Xiaogan Li
- [Anisotropic thermoelectric transport properties in polycrystalline SnSe₂](#)
Caiyun Li, , Wenke He *et al.*

Laser-induced phase conversion of n-type SnSe₂ to p-type SnSe

Qi Zheng(郑琦)^{1,2,†}, Rong Yang(杨蓉)^{1,2,4,‡}, Kang Wu(吴康)^{1,2}, Xiao Lin(林晓)^{2,3}, Shixuan Du(杜世萱)^{1,2,3,4}, Chengmin Shen(申承民)^{1,2,3}, Lihong Bao(鲍丽宏)^{1,2,3,4,‡}, and Hong-Jun Gao(高鸿钧)^{1,2,3,4,§}

¹Beijing National Center for Condensed Matter Physics and Institute of Physics, Chinese Academy of Sciences, Beijing 100190, China

²School of Physical Sciences, University of Chinese Academy of Sciences, Beijing 100190, China

³CAS Center for Excellence in Topological Quantum Computation, University of Chinese Academy of Sciences, Beijing 100190, China

⁴Songshan Lake Materials Laboratory, Dongguan 523808, China

(Received 25 October 2021; revised manuscript received 6 January 2022; accepted manuscript online 7 January 2022)

We report a facile phase conversion method that can locally convert n-type SnSe₂ into p-type SnSe by direct laser irradiation. Raman spectra of SnSe₂ flakes before and after laser irradiation confirm the phase conversion of SnSe₂ to SnSe. By performing the laser irradiation on SnSe₂ flakes at different temperatures, it is found that laser heating effect induces the removal of Se atoms from SnSe₂ and results in the phase conversion of SnSe₂ to SnSe. Lattice-resolved transmission electron microscope images of SnSe₂ flakes before and after laser irradiation further confirm such conversion. By selective laser irradiation on SnSe₂ flakes, a pattern with SnSe₂/SnSe heterostructures is created. This indicates that the laser induced phase conversion technique has relatively high spatial resolution and enables the creation of micron-sized in-plane p–n junction at predefined region.

Keywords: SnSe₂, SnSe, laser irradiation, local phase conversion

PACS: 73.63.Bd, 64.70.Nd, 42.55.Ye, 78.30.–j

DOI: 10.1088/1674-1056/ac4901

1. Introduction

In the past years, transition metal dichalcogenides (TMDs) have attracted intensive research interests due to their diverse electronic properties, such as metal/band insulators,^[1–3] semiconductors,^[3–7] charge density waves,^[8–10] ferromagnetism,^[11] valley polarization,^[12,13] etc. These versatile properties come from the diversity of their compositions and phases, including trigonal prismatic (2H), octahedral (1T), rhombohedral (3R), monoclinic (1T') phases,^[14,15] etc. Due to the weak bonding energies in metal-selenium bonds, there is a low energy requirement to lose Se in selenide minerals and the phase transition in selenide minerals is widely reported.^[16–18] Recently, an electron-beam induced phase conversion technique has been reported in which the electrons accelerated up to 300 keV in a transmission electron microscope (TEM) system gain enough energy for knocking a weak bonded atom (for example Se in PdSe₂)^[19] out of the sample and the *in-situ* TEM observation provides the possibility of understanding the phase conversion mechanism in atomic scale. Besides the mechanism study, this local phase transition technique also provides high controllability to form semiconductor homojunction when the two phases before and after conversion have different properties, such as by converting n-type to p-type semiconductor, a p–n junction can be fabricated. Compared with the traditional nanomicro fabri-

cation to prepare semiconductor p–n junctions by locally ion implantation, the local phase conversion technique is more efficient and has better controllability.

For the tin selenides, stable layered crystal phases (Fig. 1(a)) are known with Sn in Sn(IV) [SnSe₂, n-type] and Sn(II) [SnSe, p-type] oxidation states. The p–n junction of SnSe₂ and SnSe formed by local phase conversion of n-type SnSe₂ to p-type SnSe with *in-situ* electron beam irradiation in a TEM was firstly reported by P. Shutter *et al.* in 2016.^[16] After that, thermally driven conversion of n-type SnSe₂ to p-type SnSe by direct heating is developed and in-plane p–n junction has been formed.^[20] Creating in-plane p–n junctions at predefined locations is critical for further exploration of the novel properties and device applications of SnSe₂–SnSe heterostructure. Here, we report laser-induced transformations of layered tin dichalcogenides from n-type SnSe₂ to SnSe. By collecting Raman spectra on SnSe₂ flakes before and after laser irradiation, the phase conversion from n-type SnSe₂ to p-type SnSe is confirmed. The conversion mechanism of laser heating effect induced removal of Se atoms from SnSe₂ is revealed by the Raman spectra collected at different substrate temperatures and laser power levels. Lattice resolved transmission electron microscope (TEM) images confirms such conversion at atomic levels. Finally, a pattern with SnSe₂/SnSe heterostructures is created by selective laser irradiation on SnSe₂ flakes, indicating that the laser induced phase conversion technique

[†]These authors contributed equally.

[‡]Corresponding author. E-mail: lhbao@iphy.ac.cn

[§]Corresponding author. E-mail: hjgao@iphy.ac.cn

has relatively high spatial resolution and enables the creation of micron-sized in-plane p–n junction at predefined region.

2. Methods

2.1. Growth of SnSe₂ nanoflakes

The SnSe₂ nanoflakes were grown by chemical vapor deposition (CVD) on a mica substrate using Se and SnI₂ pills as precursors,^[21] as schematically shown in Fig. 1(a). The substrate was loaded into a double heating zone CVD furnace and placed 20 cm down stream to a quartz crucible containing 13.5 mg of SnI₂ ($\geq 99.999\%$, Alfa) with another quartz crucible containing 400 mg of Se ($\geq 99.999\%$, Alfa) in the upper stream. The Se pills in the first heating zone were heated up to 470 °C in advance to insure a Se rich environment. Then the SnI₂ pills were heated up to 530 °C in 10 min and kept for 15 min under a flow of 5 sccm H₂ + 20 sccm Ar carry gas. The key step to get thin and large SnSe₂ nanoflakes is fast cooling down the substrate to room temperature after the growth progress.

2.2. Sample characterization and laser irradiation progress

Optical microscope (BX51, OLMPUS) and atomic force microscope (SPA 400, SII) in tapping mode were used for characterization of the morphology and thickness of SnSe₂ flakes. TEM images and SAED pattern were taken by JEOL JEM-2100 at an accelerating voltage of 200 kV. TEM samples were prepared by directly scraping SnSe₂ flakes from the as grown substrate and collecting them on TEM grid. Laser irradiation on SnSe₂ flakes was performed by the laser in a confocal Raman/PL system (Horiba HR-Evolution) and the Raman spectra were collected *in-situ* before and after the phase conversion process. A home updated variable temperature (VT)-VACUUM Raman system (Horiba HR-800) was used for the temperature dependent conversion.

3. Results and discussion

3.1. Synthesis and characteristic of SnSe₂ nano flakes

The SnSe₂ flakes were synthesized by a CVD method.^[21] Figures 1(b) and 1(d) show the optical micrograph of the as-grown SnSe₂ flakes. The SnSe₂ flakes show either hexagonal or triangular shapes, which can be controlled by varying the substrate temperature. As shown in Fig. 1(c), the lateral size of the triangular shaped flake can reach up to $\sim 80 \mu\text{m}$. Its thickness was measured by line profile analysis of atomic force microscope (AFM). An AFM image of the SnSe₂ flake is shown in the inset of Fig. 1(c) and its thickness is measured as $\sim 2.1 \text{ nm}$. The lateral size of hexagonal SnSe₂ nano-flake can reach up to $\sim 30 \mu\text{m}$ (Fig. 1(e)). High-resolution transmission electron microscopy (HRTEM) was used to characterize the

lattice structures of the SnSe₂ nanoflakes. The lattice fringes shown in Fig. 1(f) indicate a perfect atomic structure with a lattice spacing of 3.3 \AA , corresponding to the (10 $\bar{1}$) planes of a hexagonal-phase SnSe₂.^[22] Further selected area electron diffraction (SAED) pattern also confirms the high quality and single-crystalline nature of SnSe₂, as shown in the inset of Fig. 1(f). The element analysis of Sn and Se by energy dispersive x-ray spectroscopy (EDX) study shows a 1 : 2 atomic ratio of Sn versus Se, as shown in Fig. S1. The Raman spectrum in Fig. 1(g) shows clear peaks of the E_g mode at 117 cm^{-1} and A_{1g} mode at 185 cm^{-1} , respectively, which is consistent with previous result.^[23]

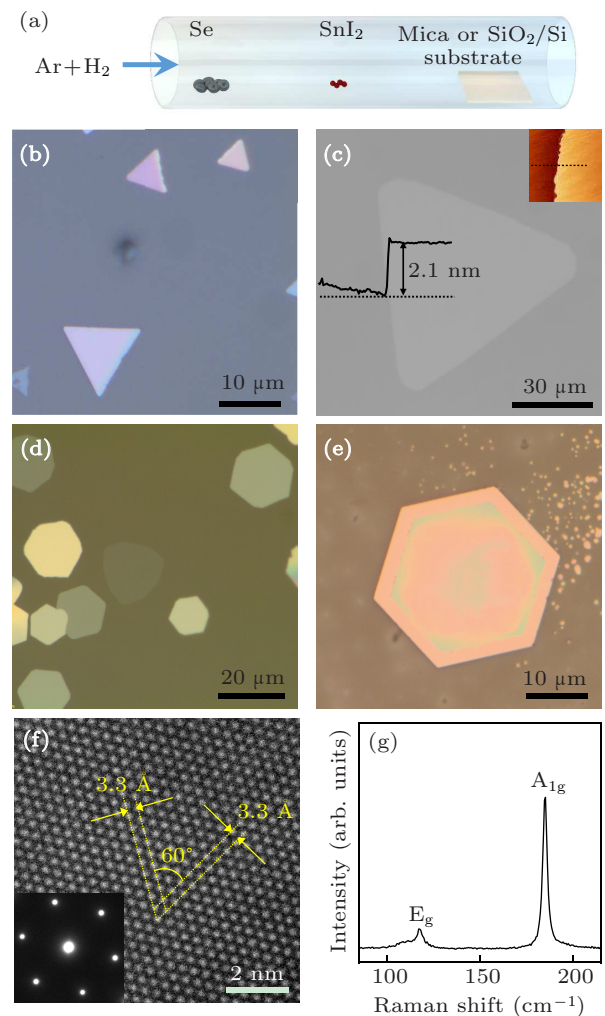


Fig. 1. Preparation and characterization of single crystalline SnSe₂ flakes. (a) Schematic diagram of the preparation of SnSe₂ flakes by CVD. (b) Optical image of triangular SnSe₂ flakes as-grown on a mica substrate. (c) Optical image of an individual SnSe₂ flake with thickness of 2.1 nm. Inset is the AFM image of the same SnSe₂ flake. (d) Optical image of hexagonal SnSe₂ flakes as-grown on a mica substrate. (e) Optical image of an individual SnSe₂ flake with hexagonal morphology. (f) Lattice-resolved TEM image of a single SnSe₂ nanoflake. Inset is the SAED image. (g) The Raman spectrum collected on a typical SnSe₂ nanoflake.

3.2. Laser induced conversion from SnSe₂ to SnSe

In Raman spectrum measurements, the Raman scatter signal increases with the gain of laser power and if high laser power is applied, the sample may be burnt by heating effect.

Figure 2(a) shows the burnt holes at top corner and right corner of a triangle SnSe₂ nanoflake after collecting Raman spectrum for 60 s with laser power of 25 mW under a 532 nm laser irradiation. To study the laser irradiation effect on the structure of SnSe₂ flake, Raman spectra were collected before and after the laser irradiation process. As shown in Fig. 2(b), the black line and red line represent the Raman signals before and after the laser irradiation progress, respectively, and the blue lines show the peaks fitting after the laser irradiation. In comparison to the Raman signal from SnSe₂, new Raman peaks located at 69 cm⁻¹, 93 cm⁻¹ and 153 cm⁻¹ emerge after the laser irradiation, which represents the A_g¹, B_{3g} and A_g³ vibration modes of SnSe crystal,^[24] respectively. This indicates that by laser irradiation on SnSe₂ flake, SnSe₂ can be converted to SnSe. In addition, the A_{1g} peak at 185 cm⁻¹ and the E_g peak at 117 cm⁻¹ of SnSe₂ remain after the laser irradiation, which indicates that SnSe₂ is not completely converted to SnSe. This is because that during laser irradiation the heat distribution of the irradiation area is not uniform. Figure 2(c) shows a simple sketch of the laser irradiation progress. The core part has a higher temperature than the edge of the outer area, so the conversion from SnSe₂ to SnSe may happen only in the core part. An AFM image of the burnt hole is shown in the upper inset of Fig. 2(c), which initially confirms that the laser heating effect might be the physical mechanism of the conversion. Furthermore, an area conversion progress is performed by point-by-point laser irradiation on SnSe₂ flake, as shown in Fig. 2(a). Figure 2(d) shows the Raman spectra collected from the area of original SnSe₂ (black), after point conversion (red) and after

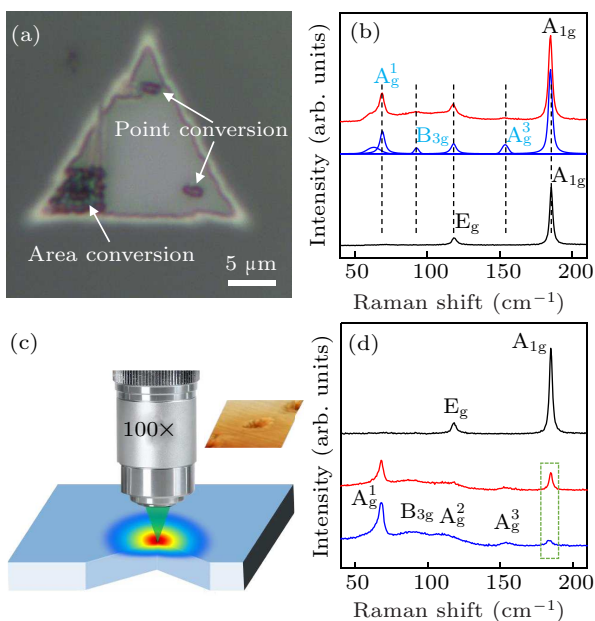


Fig. 2. Laser induced phase conversion of n-type SnSe₂ to p-type SnSe. (a) Optical microscope image of the SnSe₂ flake with point conversion and area conversion. (b) The Raman spectra before (black) and after (red) conversion together with peak fitting (blue). (c) The schematic diagram of the heat distribution during conversion and the 3D AFM image of a burnt hole (upper inset). (d) Raman spectra of original SnSe₂ (black), after point conversion (red) and area conversion (blue), respectively.

area conversion (blue), respectively. The green dashed rectangle highlights that the A_{1g} peak of SnSe₂ located at 185 cm⁻¹ is substantially reduced after area conversion, indicating that the SnSe₂ is almost completely converted to SnSe.

3.3. The temperature- and laser power-dependent conversion of SnSe₂ to SnSe

To further study the conversion mechanism, temperature- and power-dependent conversion process was performed. To exclude the influence of the thickness of SnSe₂ on the conversion efficiency, a bulk SnSe₂ single crystal was used as the sample. As shown in Fig. 3(a), under a 532 nm laser irradiation, the Raman spectra collected on the region after conversion with different laser powers suggest that only the 15 mW irradiation can completely convert SnSe₂ to SnSe. Figure 3(b) shows the Raman spectra of SnSe₂ after conversion at different temperatures with a constant laser power of 15 mW. It is clearly found that the conversion can only happen at temperatures higher than 150 K. As a constant laser power has a constant heating effect, the conversion becomes impossible when the substrate is cooling down and even the hottest center area under the laser beam cannot gain enough energy to convert SnSe₂ to SnSe. A laser with longer wavelength of 633 nm was also used to convert SnSe₂ to SnSe. As shown in Fig. 3(c), only when the laser power reaches 8.3 mW, the conversion process can occur. For the conversion at different temperatures with constant power of 8.3 mW, the conversion process can

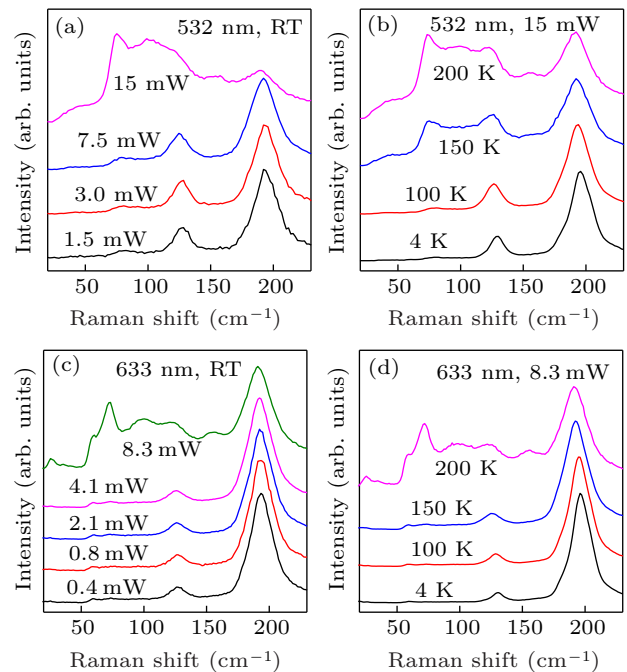


Fig. 3. Laser power- and temperature-dependent conversion of SnSe₂ to SnSe. (a) Raman spectra of SnSe₂ after a 532 nm laser irradiation with different laser powers at room temperature (RT). (b) Raman spectra of SnSe₂ after a 532 nm laser irradiation with power of 15 mW at different substrate temperatures. (c) Raman spectra of SnSe₂ after a 633 nm laser irradiation with different laser powers at RT. (d) Raman spectra of SnSe₂ after a 633 nm laser irradiation with power of 15 mW at different substrate temperatures.

only happen when the substrate temperature reaches 200 K. All these results confirm that the laser heating effect accounts for the physical mechanism of conversion of SnSe₂ to SnSe.

3.4. Patterned conversion of SnSe₂ to SnSe

HRTEM was used to further confirm that after laser irradiation, SnSe₂ is converted to SnSe. After laser irradiation, burnt holes with a diameter of 1–2 μm are clearly observed in the TEM image of SnSe₂ flake, as shown in Fig. 4(a). The lattice resolved HRTEM image of the region at the edge of the burn hole after laser irradiation is shown in Fig. 4(b). The lattice fringes indicate a perfect atomic structure with a lattice spacing of 3.02 Å, corresponding to the (011) planes of an orthogonal-phase SnSe.^[24] As discussed above, only the center region under laser irradiation can be converted. Therefore, the local conversion of SnSe₂ to SnSe at predefined regions can reach a higher spatial resolution than the laser spot. Figure 4(c) shows the AFM image of SnSe₂ flake after a 532 nm laser irradiation with power of 2 mW. The depth of burnt holes is ~ 1.5 nm and the diameter is smaller than 200 nm, which is much smaller than the diameter of the laser spot (~ 500 nm) with the 100× objective lens. To demonstrate the capability of creation of in-plane SnSe₂–SnSe p–n junction by this local phase conversion technique, patterned conversion of SnSe₂ to SnSe was performed by point-by-point laser irradiation on SnSe₂ flakes. As shown in Fig. 4(d), an “IOP” pattern is clearly observed. Lower inset shows the Raman mapping at 69 cm⁻¹ of the pattern, indicating that the irradiation area is completely converted into SnSe.

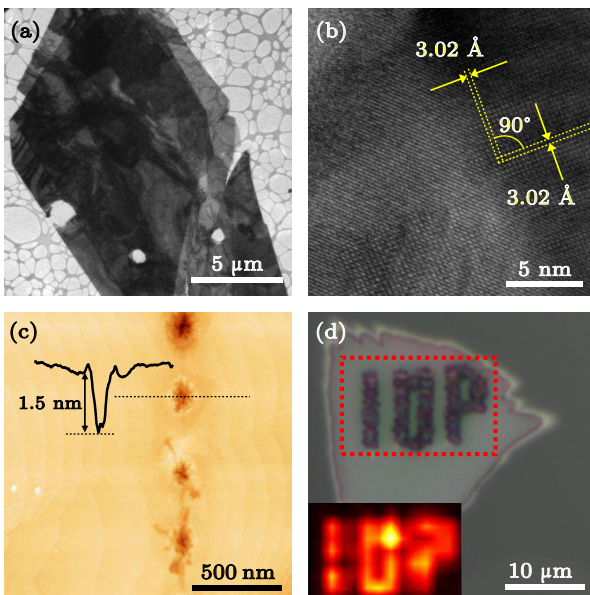


Fig. 4. (a) TEM image of the SnSe₂ flake after laser irradiation. Laser burnt holes can be clearly observed. (b) The lattice-resolved TEM image of the region at the edge of the burn hole after laser irradiation. (c) AFM image of SnSe₂ flake after a 532 nm laser irradiation with power of 2 mW. (d) Optical microscope image of SnSe₂ nanoflake after patterned laser-induced phase conversion. The lower inset shows the Raman mapping image of the pattern, indicating that the irradiation area is completely converted into SnSe.

4. Conclusion

In summary, we have developed a novel method to locally convert n-type SnSe₂ to p-type SnSe. This inversion is confirmed by collecting Raman spectra on SnSe₂ flakes before and after laser irradiation. The physical mechanism of this phase conversion is revealed by measuring the Raman spectra of SnSe₂ flakes after laser irradiation performed at different temperatures, indicating that it is the laser heating effect induces the removal of Se atoms from SnSe₂ to convert SnSe₂ to SnSe. High-resolution TEM image of SnSe₂ flakes after laser irradiation shows atomic structure of SnSe, further confirming the conversion of SnSe₂ to SnSe. The successful patterned conversion of SnSe₂ to SnSe shows that this laser induced phase conversion technique has a high spatial resolution better than the laser spot and enables the creation of micron-sized in-plane p–n junction at predefined region.

Acknowledgments

This work was supported by the National Key Research & Development Project of China (Grant Nos. 2016YFA0202300 and 2018FYA0305800), the National Natural Science Foundation of China (Grant No. 61888102), Strategic Priority Research Program of Chinese Academy of Sciences (Grant Nos. XDB30000000 and XDB28000000), and Youth Innovation Promotion Association of Chinese Academy of Sciences (Grant No. Y201902).

References

- [1] Yu X, Cheng H, Zhang M, Zhao Y, Qu L and Shi G 2017 *Nat. Rev. Mater.* **2** 17046
- [2] Wang J, Guo C, Guo W, Wang L, Shi W and Chen X 2019 *Chin. Phys. B* **28** 046802
- [3] Zeng Y, Zhang S, Li X, Ao J, Sun Y, Liu W, Liu F, Gao P and Zhang Y 2019 *Chin. Phys. B* **28** 058101
- [4] Novoselov K S, Geim A K, Morozov S V, Jiang D, Zhang Y, Dubonos S V, Grigorieva I V and Firsov A A 2004 *Science* **306** 666
- [5] Cui X, Lee G H, Kim Y D, Arefe G, Huang P Y, Lee C H, Chenet D A, Zhang X, Wang L, Ye F, Pizzocchero F, Jessen B S, Watanabe K, Taniguchi T, Muller D A, Low T, Kim P and Hone J 2015 *Nat. Nanotechnol.* **10** 534
- [6] Chu T, Ilatikhameneh H, Klimeck G, Rahman R and Chen Z 2015 *Nano Lett.* **15** 8000
- [7] Zhou Z, Wu L, Chen J, Ma J, Huang Y, Shen C, Bao L and Gao H J 2020 *Chin. Phys. B* **29** 118501
- [8] Zhu X Y, Wang S, Jia Z Y, Zhu L, Li Q Y, Zhao W M, Xue C L, Xu Y J, Ma Z, Wen J, Yu S L, Li J X and Li S C 2019 *Phys. Rev. Lett.* **123** 206405
- [9] Altvater M A, Tilak N, Rao S, Li G, Won C J, Cheong S W and Andrei E Y 2021 *Nano Lett.* **21** 6132
- [10] Song Z, Lei B, Cao Y, Qi J, Peng H, Wang Q, Huang L, Lu H, Lin X, Wang Y L, Du S and Gao H J 2019 *Chin. Phys. B* **28** 056801
- [11] Xia B, An L, Gao D, Shi S, Xi P and Xue D 2015 *CrystEngComm* **17** 6420
- [12] Withers F, Del Pozo-Zamudio O, Schwarz S, Dufferwiel S, Walker P M, Godde T, Rooney A P, Gholinia A, Woods C R, Blake P, Haigh S J, Watanabe K, Taniguchi T, Aleiner I L, Geim A K, Fal'ko V I, Tartakovskii A I and Novoselov K S 2015 *Nano Lett.* **15** 8223
- [13] Zhao Y, Bo T, Du L, Tian J, Li X, Watanabe K, Taniguchi T, Yang R, Shi D, Meng S, Yang W and Zhang G 2021 *Chin. Phys. B* **30** 057801
- [14] Wang Q H, Kalantar-Zadeh K, Kis A, Coleman J N and Strano M S 2012 *Nat. Nanotechnol.* **7** 699

- [15] Manzeli S, Ovchinnikov D, Pasquier D, Yazyev O V and Kis A 2017 *Nat. Rev. Mater.* **2** 17033
- [16] Sutter E, Huang Y, Komsa H P, Ghorbani-Asl M, Krasheninnikov A V and Sutter P 2016 *Nano Lett.* **16** 4410
- [17] Fan P, Qian G, Wang D, Li E, Wang Q, Chen H, Lin X and Gao H J 2021 *Chin. Phys. B* **30** 018105
- [18] Li E, Zhang R Z, Li H, Liu C, Li G, Wang J O, Qian T, Ding H, Zhang Y Y, Du S X, Lin X and Gao H J 2018 *Chin. Phys. B* **27** 086804
- [19] Lin J, Zuluaga S, Yu P, Liu Z, Pantelides S T and Suenaga K 2017 *Phys. Rev. Lett.* **119** 016101
- [20] Tian Z, Zhao M, Xue X, Xia W, Guo C, Guo Y, Feng Y and Xue J 2018 *ACS Appl. Mater. Interfaces* **10** 12831
- [21] Xue M, Zheng Q, Chen R, Bao L, Du S and Chen J 2019 *Nanoscale* **11** 14113
- [22] Fang Z, Hao S H, Long L Y, Fang H, Qiang T T and Song Y X 2014 *CrystEngComm* **16** 2404
- [23] Pei T, Bao L, Wang G, Ma R, Yang H, Li J, Gu C, Pantelides S, Du S and Gao H J 2016 *Appl. Phys. Lett.* **108** 053506
- [24] Pei T, Bao L, Ma R, Song S, Ge B, Wu L, Zhou Z, Wang G, Yang H, Li J, Gu C, Shen C, Du S and Gao H J 2016 *Adv. Electron. Mater.* **2** 1600292